Anal Bioanal Chem (2016) 408:2083–2093
DOI 10.1007/s00216-015-9298-6

RESEARCH PAPER

Fluorescent molecularly imprinted polymer based on *Navicula* sp. frustules for optical detection of lysozyme

Guat Wei Lim[1] · **Jit Kang Lim**[1,2] · **Abdul Latif Ahmad**[1] · **Derek Juinn Chieh Chan**[1]

Received: 30 September 2015 / Revised: 21 December 2015 / Accepted: 23 December 2015 / Published online: 3 February 2016

Abstract The direct correlation between disease and lysozyme (LYZ) levels in human body fluids makes the sensitive and convenient detection of LYZ the focus of scientific research. Fluorescent molecularly imprinted polymer has emerged as a new alternative for LYZ detection in order to resolve the limitation of immunoassays, which are expensive, unstable, require complex preparation, and are time consuming. In this study, a novel fluorescence molecularly imprinted polymer based on *Navicula* sp. frustules (FITC-MIP) has been synthesized via post-imprinting treatment for LYZ detection. *Navicula* sp. frustules were used as supported material because of their unique properties of moderate surface area, reproducibility, and biocompatibility, to address the drawbacks of nanoparticle core material with low adsorption capacity. The FITC acts as recognition signal and optical readout, whereas MIP provides LYZ selectivity. The synthesized FITC-MIP showed a response time as short as 5 min depending on the concentration of LYZ. It is found that the LYZ template can significantly quench the fluorescence intensity of FITC-MIP linearly within a concentration range of 0 to 0.025 mg mL^{-1}, which is well described by Stern-Volmer equation. The FITC-MIP can selectively and sensitively detect down to 0.0015 mg mL^{-1} of LYZ concentration. The excellent sensing performance of FITC-MIP suggests that FITC-MIP is a potential biosensor in clinical diagnosis applications.

Keywords Fluorescent · Molecularly imprinted polymer · *Navicula* sp. frustules · FITC · Lysozyme recognition

Electronic supplementary material The online version of this article (doi:10.1007/s00216-015-9298-6) contains supplementary material, which is available to authorized users.

✉ Derek Juinn Chieh Chan
chderekchan@usm.my

[1] School of Chemical Engineering, Engineering Campus, Universiti Sains Malaysia, Seri Ampangan, 14300 Nibong Tebal, Seberang Perai Selatan, Pulau Pinang, Malaysia

[2] Department of Physics, Carnegie Mellon University, Pittsburgh, PA 15213, USA

Introduction

Lysozyme (LYZ) has widespread distribution in both animals and plants [1]. In humans, LYZs are present in tears, milk, saliva, serum, urine, and other body fluids [2]. These LYZs in human body fluid could be used as an important index in the diagnosis of various diseases [3]. For instance, the concentration of LYZ in serum of a healthy human is about 0.0017 mg mL^{-1} [2]. However, the serum LYZ level can be significantly elevated to 0.015 mg mL^{-1} in patients who are suffering from leukemia [4–6], renal disease [7], and sarcoidosis [2]. In addition, LYZ was usually not detectable in the cerebrospinal fluid of normal individual [8] but was found to be present in concentration of about 0.0055 mg mL^{-1}, 0.010 mg mL^{-1}, and 0.0037 mg mL^{-1} during the course of bacterial meningitis, pneumococcal meningitis, and tuberculous meningitis, respectively [9].

Traditionally, it is very difficult to detect LYZs, which act as biomarkers for disease diagnosis from complex protein mixture [10]. The conventional immunoassay that employs antibodies, enzymes, immunoglobulins, and other biological compounds as recognition elements have demonstrated an excellent level of sensitivity and selectivity. However, they suffer from several fundamental limitations, including physiochemical instability, complex preparation method, are expensive, time-consuming, and require experienced operators to perform the test. This hampered their widespread used in

biosensors [10–12]. In this respect, an alternative artificial biomimetic receptor, such as molecularly imprinted polymer, exhibits the potential to be applied in the field of protein recognition as it is easily prepared with low cost, has good mechanical and chemical stability and can be stored easily [13]. Among several reported molecularly imprinted polymer techniques, surface imprinting onto core material is particularly suitable for bulky structure template such as protein, as the transport problem can be alleviated [14]. Recently, several research groups have synthesized molecularly imprinted polymer onto silica nanoparticles [14–18] and magnetic nanoparticles [19–22] for selective recognition of protein. Although the resulting imprinted polymer layer demonstrated high selectively towards protein template associated with the fast adsorption kinetics, the specific rebinding capacities are still unsatisfactory, and this limits the sensitivity of assay. In addition, even though the molecularly imprinted polymer can selectively recognize protein template, the template that has bonded at the recognition sites must be removed and then detected via an expensive and complicated technique, such as high-liquid chromatography (HPLC) [23]. Hence, it is still a difficult task to prepare molecularly imprinted polymer that can be applied to specifically recognize and directly quantify the protein template without extracting the template from polymer matrix and, hence, making the quantification very time-consuming and complicated.

Fluorescence offers an attractive alternative for identification and quantification of biological compounds, requiring less preparation time and without compromising sensitivity [24, 25]. The incorporation of fluorescence signal could greatly enhance the utility of the molecularly imprinted polymer without sacrificing the selectivity of developed molecularly imprinted polymer [26, 27]. Among various types of fluorophore, fluorescein isothiocyanate isomer I (FITC) has drawn numerous research efforts and has been widely used in microorganism staining and labeling [28–30] and fluorescence immunoassays [31] because of its high solubility in water, high quantum efficiency, and large extinction coefficient [32]. In recent years, various forms of FITC-labeled molecularly-imprinted polymer, relying on the use of fluorescence quenching, have been prepared. For instance, Huang et al. (2013) have synthesized the FITC-labeled molecularly imprinted polymer on magnetic nanoparticles as recognition material towards bisphenol A [33]. Subsequently, Chen et al. (2014) has prepared FITC functionalized magnetic core-shell Fe_3O_4/Ag hybrid nanoparticles for detection of molecular biothiols [34]. Furthermore, Feng et al. (2014) developed FITC-labeled molecularly imprinted polymer on silica nanoparticles for detection of perfluorooctane sulfonate [35]. Then, Wang et al. (2015) developed FITC-labeled molecularly imprinted polymer on silica beads that are capable of selective recognition and fluorescence detection of λ-cyhalothrin [24]. In addition, FITC-labeled protein configuration based on a modulation of plasmon-enhanced resonance energy transfer to gold nanoparticles by protein shell gating for detection of proteins, including cytochrome *c*, bovine serum albumin, and survivin were achieved by Stobiecka and Chalupa [36, 37]. These developed FITC-labeled molecularly imprinted polymers can not only can with template selectively, but also can generate detectable optical signals for visualization after the templates have been bound. As seen, the molecularly imprinted polymer coupled with fluorescence is a more convenient and effective strategy for detecting the target molecules with excellent merits. Nevertheless, reports on FITC-based MIP sensors for protein detection are scarce [26].

In this study, a fluorescent molecularly imprinted polymer for selective and quantitative detection of LYZ was constructed by incorporating FITC to newly designed molecularly imprinted polymer based on *Navicula* sp. frustule (diatom frustule) as a new core material [38]. The frustule possesses unique characteristics of highly organized nanostructured pores, reproducible with exactness in massive numbers, moderate surface area (20–100 $m^2\ g^{-1}$), and easily found in fresh and salt water [39–42]; it exhibited enhancement in rebinding capacity of molecularly imprinted polymer without showing significant decrease in adsorption kinetics [38]. The FITC anchored on molecularly imprinted polymer by covalent bonding with acrylamide functional monomers via post-imprinting treatment (Fig. 1). The signal transduction of protein binding on FITC-MIP was evaluated by measuring the fluorescence spectral change. The response of the intensity of fluorescence signal and application capability of FITC-MIP were carried out in a series of experiments, including binding study, kinetics study, selectivity study, as well as stability study.

Experimental

Synthesis of FITC-MIP and FITC-NIP

Pristine *Navicula* sp. frustules were obtained through chemical cleaning of monoculture of *Navicula* sp., which was cultured in artificial seawater using Conway medium at 25 °C under continuous aeration and illumination of 20–30 μmol photons $m^{-2}.s^{-1}$ [43]. The LYZ imprinted polymer (denoted MIP) and nonimprinted polymer (denoted NIP) were prepared on *Navicula* sp. frustules by radical induced graft copolymerization method as reported in our previous work [38]. Subsequently, the fluorescent-LYZ imprinted frustules (denoted FITC-MIP) were prepared through post-imprinting treatment, in which 0.1 g of fluorescein isothiocyanate (FITC) was added to the flask containing 10 mL of ethanol (purity ≥ 99.5 %) followed by addition of 0.1 g of MIP. The mixture was reacted for 24 h at room temperature under continuous magnetically stirring. The flask was wrapped with aluminium foil to prevent

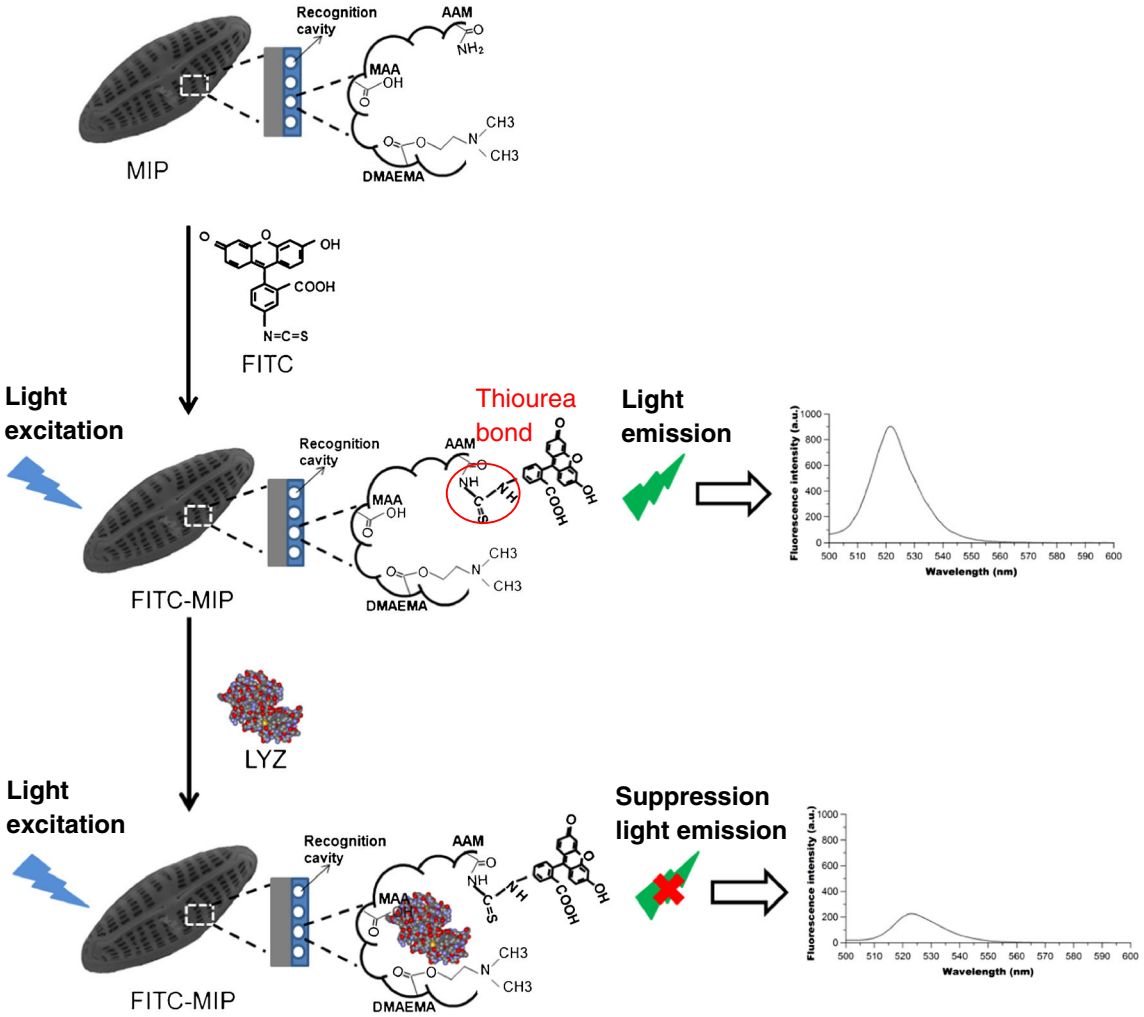

Fig. 1 Illustration for preparation of FITC-MIP and the fluorescence quenching detection of LYZ upon specific recognition

FITC photo-bleaching during the entire reaction process. The FITC-MIP was collected by centrifugation at 3500 × *g*, and washed several times with ethanol and deionized water to remove unreacted FITC. Finally, the FITC-MIP was dried by freeze-drying for 24 h. The preparation of FITC-MIP and protein detection mechanism is illustrated in Fig. 1. The fluorescent nonimprinted frustules (denoted FITC-NIP) were prepared and washed in the same way as FITC-MIP.

Characterization

Fluorescent measurements were performed with Perkin Elmer, Waltham, MA, USA, LS55 fluorescent spectrophotometer equipped with 1 cm quartz cuvette at 25 °C, with excitation wavelength (λ_{ex}) and emission wavelength (λ_{em}) of 498 nm and 522 nm, respectively. The slit widths of excitation and emission were 5 nm. The functional groups on the prepared samples were determined using a Thermo Scientific, Waltham, MA, USA, Nicolet iS10 FTIR spectrometer. The Fourier transform infrared (FTIR) spectra were recorded over the range of 4000 to 650 cm^{-1}. The fluorescence images of FITC-MIP and FITC-NIP were examined under fluorescence microscope (Olympus BX53). The excitation and emission filter set used was 470-490/520 nm (U-FBW; Olympus, Tokyo, Japan). Fluorescence images were acquired using the computer software CellSens Dimension (Olympus). In addition, Ultraviolet-visible (UV-Vis) spectra of LYZ, FITC-MIP and FITC-NIP were recorded within the range of 200–800 nm on a UV-Vis spectrophotometer (Agilent Technologies, Cary 60).

Sensing performance of FITC-MIP and FITC-NIP

Effect of pH

To examine the pH effect at 25 °C, FITC-MIP and FITC-NIP were dispersed in buffer solution with pH varied from 3 to 10. The fluorescence intensity value from fluorescence spectra was recorded by fluorescence spectrophotometer (λ_{ex} = 498 nm, λ_{em} = 522 nm). Each measurement was performed in triplicate and mean values are presented.

Binding studies for different LYZ concentration

The binding properties of FITC-MIP and FITC-NIP were investigated by equilibrium binding experiments with fluorescence measurements; 1.5 mg of FITC-MIP was added to 10 mL of LYZ solution (pH 7, 10 mM) with concentration of 0.002 mg mL^{-1} in a 20-mL glass vial. The glass vial was wrapped in aluminium foil and incubated for 1 h at 25 °C on an end-to-end rotating mixer with a speed of 40 rpm. Then the fluorescence intensity of the solution was measured using fluorescent spectrophotometer (λ_{ex} = 498 nm, λ_{em} = 522 nm). The fluorescence quenching efficiency of the FITC-MIP with LYZ was calculated by Stern-Volmer equation:

$$\frac{I_0}{I} = 1 + K_{SV}C \quad (1)$$

where I_0 is the initial fluorescence intensity in the absence of LYZ template, I is the fluorescence intensity in the presence of LYZ, *Ksv* (mL g^{-1}) is the Stern-Volmer quenching constant, and C (mg mL^{-1}) is the concentration of LYZ. The assay was also carried out using LYZ solution at concentrations ranging from 0 to 0.05 mg mL^{-1}. The same procedure was performed for FITC-NIP. All the experiments were carried out in triplicate at each LYZ concentration.

Binding kinetics experiment

The binding kinetics study was carried out using the same experimental procedure as in binding studies for different LYZ concentration. At preset intervals of time, the fluorescence intensity of the solution was monitored and recorded using a fluorescent spectrophotometer (λ_{ex} = 498 nm, λ_{em} = 522 nm). The experiment was continued until equilibrium conditions were reached where no further intensity quenching was detected. All the described experiments were done in triplicate with the average value reported.

Selectivity and competitive binding studies

To measure the selectivity of FITC-MIP, a fluorescence quenching comparison was made between the competitive proteins [bovine serum albumin (BSA) and cytochrome *c* (Cyt C) and LYZ]. It was performed by adding 1.5 mg of FITC-MIP into 10 mL of protein solutions containing 0.007 mg mL^{-1} of LYZ, BSA, or Cyt C at pH 7. The mixture was incubated for 1 h at 25 °C in darkness. After that the fluorescence spectrum were detected by fluorescence spectrophotometer (λ_{ex} = 498 nm, λ_{em} = 522 nm). To further evaluate the selectivity of FITC-MIP in the presence of competitive proteins, BSA and Cyt C were added into 10 mL of LYZ solution at different concentration ratios of LYZ/Cyt C/BSA (1/0/0 to 1/5/5). The amount of FITC-MIP and LYZ concentration was fixed at 1.5 mg and 0.007 mg mL^{-1}, respectively. After adsorption was completed, the fluorescence spectra of the solution was analyzed using fluorescence spectrophotometer (λ_{ex} = 498 nm, λ_{em} = 522 nm). The same procedure was carried out by replacing FITC-MIP with FITC-NIP. All the experiments were run in triplicate and mean values are reported.

Fluorescence stability study

The stability of FITC-MIP was also studied by adding 1.5 mg of FITC-MIP to 10 mL phosphate buffer solution (pH 7, 10 mM) and the fluorescent intensity of the solution was monitored using fluorescence spectrophotometer (λ_{ex} = 498 nm, λ_{em} = 522 nm) every 1 h for 8 h duration. Then, the change of fluorescence intensity during the storage of FITC-MIP (stored at 4 °C in a dark environment) was also investigated for a 1-mo period. All the measurements were taken three times and the average values are presented.

Results and discussion

Preparation and characterization of FITC-MIP and FITC-NIP

The design of FITC-MIP is based on the fact that FITC acted as recognition signal transducer and optical readout whereas MIP provides LYZ selectivity and prevents interfering molecules from coming into contact. The schematic on the preparation of FITC-MIP is shown in Fig. 1. MIP was prepared using three functional monomers formulations, namely acrylamide (AAM), methacrylic acid (MAA), and 2-(dimethylamino) ethyl methacrylate (DMAEMA), to imprint LYZ on pristine *Navicula* sp. frustules by radical induced graft copolymerization method described in our previous work [38]. FITC was introduced into MIP through post-imprinting treatment in order to transform the recognition sites of MIP into fluorescence signal that could respond to binding events. The general concept of this approach is that FITC is incorporated into MIP by reaction of amino group of AAM with FITC, forming a stable thiourea bond as seen in Fig. 1 [44]. Subsequently, the LYZ templates are entrapped in polymer matrix through noncovalent bindings (van der Waals forces and electrostatic forces). The positively charged monomer, DMAEMA, targets negatively charged amino acid (aspartic acid and glutamic acid), whilst negatively charged monomer, MAA, targets positively charged amino acid (lysine, arginine, and histidine) of LYZ template [45], which leads to fluorescence quenching.

To understand the fluorescence quenching attributable to LYZ binding, the mechanism was investigated. The resultant LYZ binding into recognition cavities in the polymer matrix

can quench the fluorescence emission of FITC through two possible pathways, namely, energy transfer and electron transfer from FITC to LYZ. As shown in the absorption spectra (Fig. 2), the absorption peak of LYZ is at 280 nm, whereas the absorption peak (almost similar to exCitation band) of FITC-MIP and FITC-NIP is located at 480 nm. It is clear that the absorption band of LYZ is located far away from the excitation band of FITC-MIP and FITC-NIP. The possible mechanism of resonance energy transfer for the fluorescence quenching is excluded in this system since there are no spectral overlaps between the absorption spectra of LYZ and the excitation spectra of FITC-MIP and FITC-NIP [26, 46]; hence, the excitation energy is unlikely to transfer from FITC to LYZ. As a result, the mechanism of fluorescence quenching can be described as a photo-induced electron transfer process [46, 47]. The electrons within the FITC first in an excited state under photo-irradiation [48]. When LYZ is present, the electrons of FITC could transfer to the lowest unoccupied molecular orbital of LYZ (see Electronic Supplementary Material (ESM) Fig. S1) [10]. This results in hindrance of electrons transition to the ground state (emitting photons and causing fluorescence) [48] and formation of neutral and cationic forms of FITC, hence quenching the fluorescence emission of FITC [47].

The FTIR spectra of the pristine *Navicula* sp. frustules, MIP, NIP, FITC-MIP, and FITC-NIP, can confirm the successful modification of frustules surface. As demonstrated in ESM Fig. S2, pristine frustules displayed the characteristic signals of bending vibration mode of inter-tetrahedral Si–O–Si bonds at 795 cm^{-1} and Si–O stretching of silanol (Si–OH) groups at 950 cm^{-1} [49]. The strong and broad peak around 1050 cm^{-1} indicated the stretching and bending vibration modes of the SiO_4 tetrahedron [49]. These peaks illustrated that pristine *Navicula* sp. frustules consisted of mainly silica [50]. In addition, these three peaks with relatively lower intensities were also observed in MIP, NIP, FITC-MIP, and FITC-NIP, suggesting that silica is present as the core material. Compared with the FTIR spectra of pristine frustules (Fig. 3), MIP and NIP displayed the absorption peak at 1651 cm^{-1} (C=O stretch), and its shoulder peak at 1615 cm^{-1} (N–H bending) verifies the presence of AAM in the polymer matrix [51, 52]. The presence of absorption peak at 1550 cm^{-1} suggested the C=O stretch from bound carboxylic acid groups, which indicates that the polymer matrix contains MAA [51, 52]. The peaks at 1720 cm^{-1} (C=O) is the contribution of DMAEMA in the polymer [51, 52]. The C–N stretching vibration band at 1147 cm^{-1} supports the presence of DMAEMA [51, 52]; however, this peak is not noticeable due to overlapping with the peak of 1050 cm^{-1} (stretching and bending vibration modes of the SiO_4 tetrahedron). These result indicated that the polymer layer consisted of three functional monomers (AAM, MAA, and DMAEMA) have been grafted on *Navicula* sp. frustules.

The FTIR spectra of FITC-MIP and FITC-NIP (Fig. 3) show a small peak located in the region of 2360 cm^{-1} corresponds to –N=C=S [53]. FITC contains an aromatic keto group, the presence of which can be manifested by the presence of a peak 1727 cm^{-1} [53, 54]. In addition, a number of peaks have been found in the carbonyl region, probably due to the presence of carbonyl group of carboxylate anion, which is authenticated by a peak near 1390 cm^{-1} resembling the characteristic peak for COO^- bending [53]. Furthermore, the absorption peaks at 1458, 1535, 1594, and 1610 cm^{-1} were assigned to characteristic peaks of the benzene ring stretching vibration [24, 54], C=O stretching vibration of amide at 1651 cm^{-1} [24], along with the presence of aromatic –OH at 3163 cm^{-1} [53] indicating that the FITC had successfully bonded on both MIP and NIP.

The fluorescence property of FITC-MIP and FITC-NIP was characterized by fluorescence microscope (see ESM Fig. S3). The fluorescence of FITC-MIP and FITC-NIP was clearly observed, which indicated that the FITC was indeed successfully attached to the polymer matrix.

Sensing performance testing, effect of pH

As depicted in Fig. 4, the fluorescence intensity of FITC-MIP decreases when pH is below 6, and then it remains almost constant in the range of pH 6 to 10. FITC-NIP exhibits similar

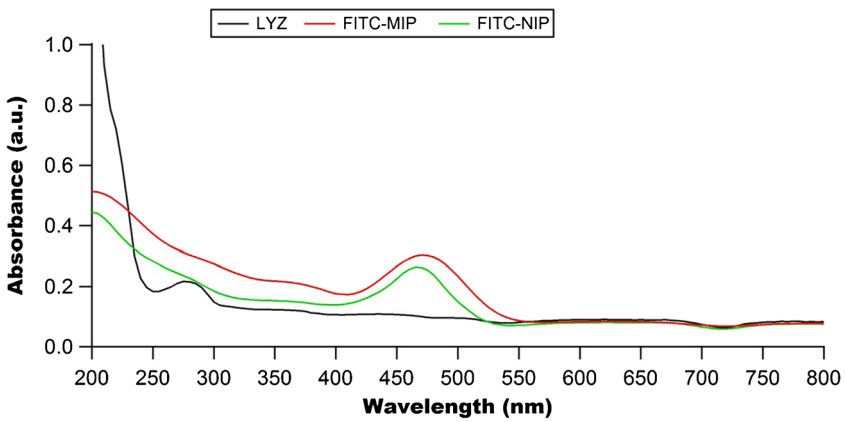

Fig. 2 Absorption spectra of LYZ, FITC-MIP and FITC-NIP in phosphate buffer (10 mM, pH 7.0)

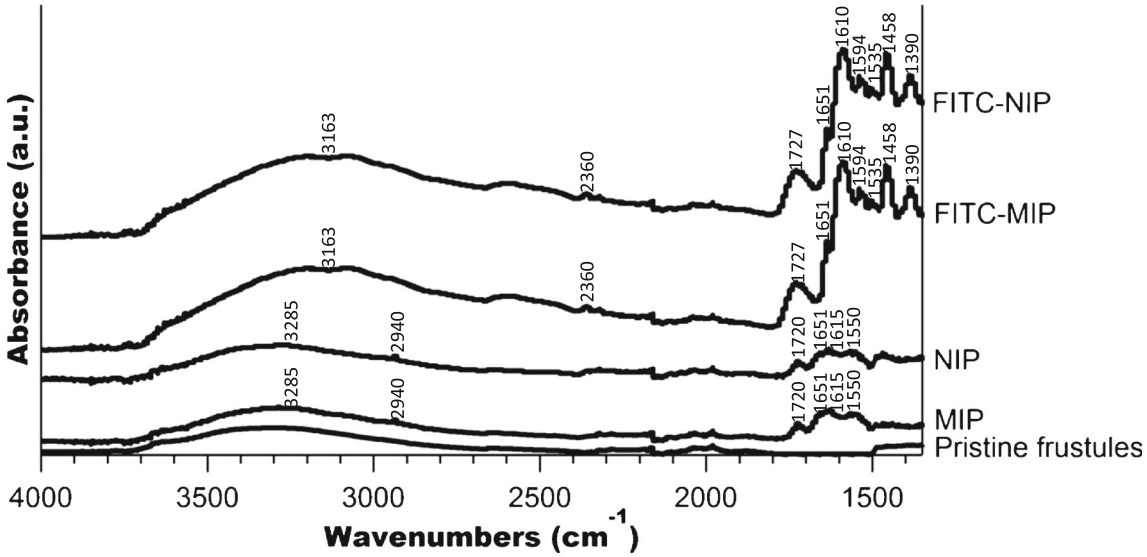

Fig. 3 FTIR spectrum of the pristine *Navicula* sp. frustules, MIP, NIP, FITC-MIP, and FITC-NIP from the range of 4000 to 1350 cm^{-1}

characteristic in response to pH values changes (see ESM Fig. S4). FITC-MIP and FITC-NIP are sensitive to pH changes because FITC appears in various ionic and neutral forms, for example cationic, neutral, anionic, and dianionic forms depending on pH values of solution [55]. The dianionic form is the most strongly fluorescing form followed by the anionic forms [56]. The neutral and cationic forms fluoresce as a result of deprotonation upon excitation converted into anion, but less intense [56]. Assuming these four species coexist in the range of pH 3–10, with different concentrations for each pH. When pH of solution is decreased, the emission intensity of FITC decreases greatly, mainly attributed to the dominant formation of neutral and cationic forms since they give lower intensity fluorescence. On the other hand, at pH 6 and above, the anionic and dianionic forms are dominative. Therefore, they give intense fluorescence intensity within this pH range. It has been established that the pH of human body fluids can be as low as 6 for saliva and as high as 8 for pancreatic fluid. As a result, the developed FITC-MIP can be utilized for quantitative fluorescent measurement for human body fluids as it is insensitive to pH over this range.

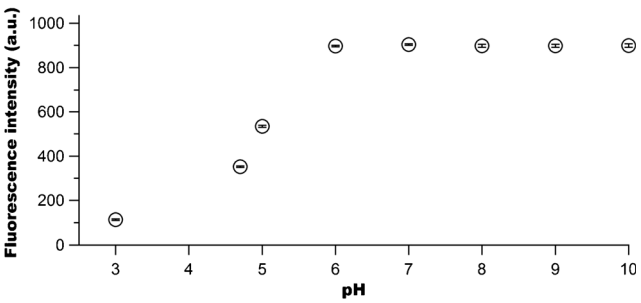

Fig. 4 The fluorescence intensity of FITC-MIP in buffers with pH ranging from 3 to 10. The points represent mean values of three replicates of measurements and error bars represent standard errors

Binding studies for different LYZ concentration

The fluorescence intensity of FITC-MIP and FITC-NIP are quenched gradually with the increasing concentration of LYZ (Fig. 5a, b). The decrease of fluorescence intensity of FITC-MIP was notably larger than that of FITC-NIP at the same concentration of LYZ. For FITC-MIP, the fluorescence quenching is mainly achieved because of the interaction of recognition sites with LYZ template [10]. In the case of FITC-NIP, the functional groups do exist but there is no specific recognition site located in polymer matrix; hence, the LYZ only has weak interaction with FITC-NIP, which results in no obvious changes of fluorescence intensity of FITC-NIP in binding process [10]. In addition, the fluorescence intensities of FITC-MIP and FITC-NIP are important data to evaluate their sensitivity [24]. The fluorescence intensity of FITC-NIP that changed with smaller amplitude than FITC-MIP suggests that FITC-NIP is less sensitivity than FITC-MIP.

Moreover, the fluorescence quenching could be further analyzed using Stern-Volmer equation. As seen in Fig. 6, the LYZ concentration range from 0 to 0.025 mg mL^{-1} has a good linear correlation with fluorescence intensity. The linear equation of FITC-MIP is $I_0/I\text{-}1 = 110.53C – 0.1577$ and the corresponding correlation coefficient (R^2) is 0.9885. The limit of detection FITC-MIP is evaluated using $3\sigma/S$, and is found to be 0.0015 mg mL^{-1}, where σ is the standard deviation of blank signal and S is the slope of the Stern-Volmer plot in Fig. 6. It is also noticed that detection range of LYZ concentration for FITC-MIP is 0 to 0.025 mg mL^{-1}. When the concentration is greater than 0.025 mg mL^{-1}, the fluorescence quenching almost reaches saturation. Similarity, the fluorescence quenching of FITC-NIP followed the Stern-Volmer equation in which the fluorescence intensity of FITC-NIP

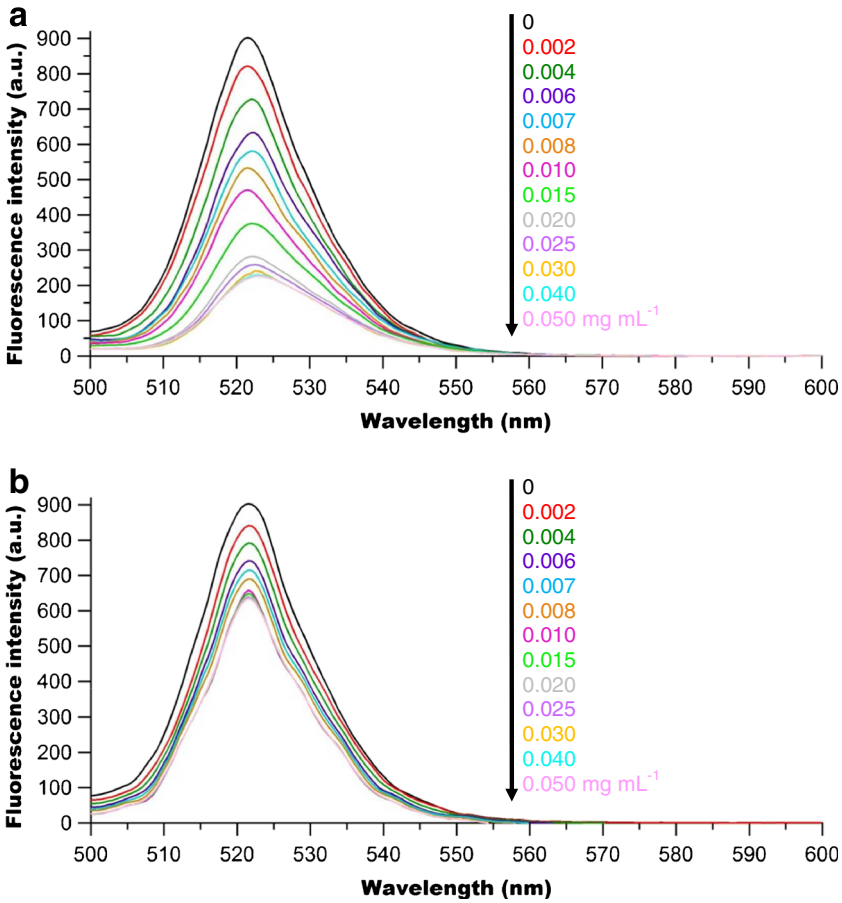

Fig. 5 Fluorescence emission spectra of the (**a**) FITC-MIP and (**b**) FITC-NIP with increasing LYZ concentration in PBS solution. Adsorption conditions: $V = 10$ mL, $W = 1.5$ mg, time 1 h, temperature 25 °C, phosphate buffer (10 mM, pH 7.0)

decreased linearly with increasing LYZ concentration from 0 to 0.01 mg mL^{-1} (Fig. 6); surpassing this range, the quenching is no longer apparent. The linear equation of FITC-NIP is $I_0/I\text{-}1 = 38.11C\text{-}0.0028$ with R^2 equal to 0.9963. Furthermore, the values of *Ksv* are determined to be 110.53 and 38.11 mL mg^{-1} for fluorescent FITC-MIP and FITC-NIP, accordingly. Additionally, the values of imprinting factor ($K_{sv,MIP}/K_{sv,NIP}$) was calculated to be 2.90 of LYZ for fluorescent FITC-MIP, which proved the successful creation of LYZ recognition cavities on FITC-MIP.

Binding kinetics study

To use the FITC-MIP as sensing material, the binding kinetics is a high interest experiment to predict the required time for analyte adsorption to reach equilibrium. The binding kinetics depends on the accessibility of the recognition site and interaction between functional groups of polymer and analyte [57]. As shown in Fig. 7, there is an immediate decrease in fluorescence intensity after the addition of LYZ. At LYZ concentration of 0.007 mg mL^{-1}, FITC-MIP shows a significant initial decrease in fluorescence intensity, but it took 15 min to obtain stable fluorescence intensity, suggesting that the rebinding equilibrium has been reached. On the other hands, it takes only about 10 min for FITC-NIP to obtain stable intensity, which was higher than the stable intensity point of FITC-MIP, indicating a weaker quenching because FITC-NIP does not have a selective binding site for LYZ. FITC-MIP takes a longer time to reach equilibrium than FITC-NIP, suggesting that FITC-MIP possessed a specific recognition site for LYZ and this caused LYZ template binding in longer time. Figure 7 also shows that the time to reach equilibrium adsorption increases gradually with the increase in concentration of LYZ. The results show that the

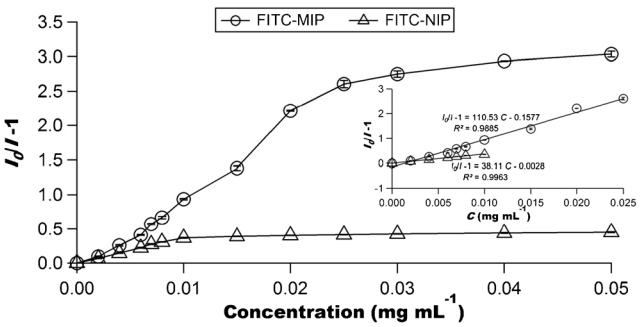

Fig. 6 Fluorescence quenching efficiency for FITC-MIP and FITC-NIP according to LYZ concentrations. The insets show the Stern-Volmer plots for respective samples. The points represent mean values of three replicates of measurements and error bars represent standard errors

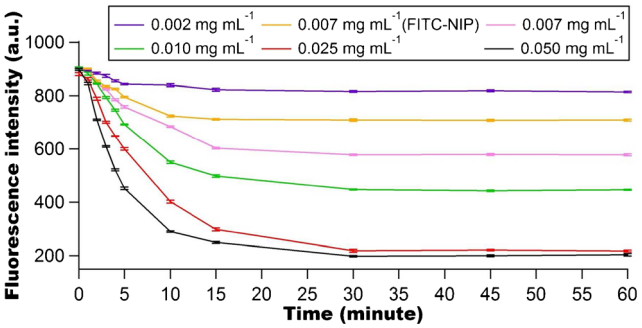

Fig. 7 Binding kinetic of FITC-MIP at varying LYZ concentration and FITC-NIP at LYZ concentration of 0.007 mg mL^{-1}. Adsorption conditions: $V = 10$ mL, $W = 1.5$ mg, temperature 25 °C. The points represent mean values of three replicates of measurements and error bars represent standard errors

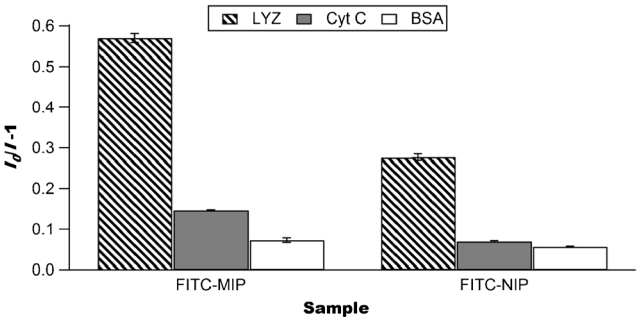

Fig. 8 Fluorescence quenching efficiency for **(a)** FITC-MIP and **(b)** FITC-NIP towards different proteins. Adsorption conditions: $V = 10$ mL, $W = 1.5$ mg, $C_{0,\,LYZ} = C_{0,\,BSA} = C_{0,\,Cyt\ C} = 0.007$ mg mL^{-1}, time 1 h, temperature 25 °C, phosphate buffer (10 mM, pH 7.0). The points represent mean values of three replicates of measurements and error bars represent standard errors

time to reach equilibrium is about 5 min for LYZ at a concentration of 0.002 mg mL^{-1}, and 30 min for LYZ at concentrations of 0.01 mg mL^{-1} and above. The response time of FITC-MIP (within 30 min) is shorter than that demonstrated in literature, in which the synthesized fluorescence MIP required 300 min [58] to achieve LYZ binding equilibrium. The fast binding kinetics in this study can be attributed to the noncovalent interaction (van der Waals and electrostatic forces) between LYZ and recognition cavities [26].

Selectivity and competitive studies

The fluorescence quenching efficiency of FITC-MIP and FITC-NIP toward various proteins was measured to study its selectivity towards template LYZ. As shown in Fig. 8, FITC-MIP had a strong response to LYZ, which caused a higher fluorescence quenching efficiency than that of BSA and Cyt C. This shows that the FITC-MIP exhibits very favorable affinity towards the template LYZ compared with nontemplate proteins (BSA or Cyt C). In the process of synthesis MIP, specific imprinted cavities with the memory of shape, size, and functional groups of LYZ were generated [59]. BSA is much larger than LYZ in molecular weight and size, so the access of BSA to recognition sites is limited by steric hindrance of polymer matrix. For Cyt C, although its molecular weight and size are close to LYZ, the functionality is not complementary to recognition cavities. This kind of nonspecific adsorption was not stable, so it was unlikely to quench significantly the fluorescence of the FITC-MIP. This is expected since BSA and Cyt C are the nontemplate proteins and their adsorption onto the FITC-MIP is attributed to nonspecific interaction. It also can be seen that the fluorescence quenching efficiency of FITC-NIP is insignificant for LYZ, Cyt C, and BSA. This indicated that there are no selective recognition sites left in FITC-NIP as FITC-NIP is prepared without addition of LYZ template molecules.

A series of ternary protein solutions of LYZ/Cyt C/BSA were prepared to study the competitive binding ability of FITC-MIP and FITC-NIP. The experiments were performed by fixing the concentration of LYZ and increasing the concentration of Cyt C and BSA at the same time. As shown in Fig. 9a, increase of LYZ/Cyt C/BSA ratio does not influence the fluorescence intensity of FITC-MIP significantly. FITC-MIP could only specifically adsorb LYZ template because of the existence of complementary recognition sites. It is difficult for BSA and Cyt C to adsorb onto it even at a high concentration. Hence, the fluorescence intensity of FITC-MIP does not change significantly if the concentration of LYZ remains the same while the concentration of Cyt C and BSA increases. These results imply the highly selective recognition ability of the FITC-MIP as it can detect the target LYZ from complex samples well. As for FITC-NIP (Fig. 9b), BSA and Cyt C did not interfere with the fluorescence intensity significantly.

Stability studies

The fluorescence stability of FITC-MIP was evaluated by repeated detection of fluorescence intensity every 1 h. As shown in Fig. 10, the change of fluorescence intensity of FITC-MIP was insignificant, which showed that emission of FITC-MIP was stable within 8 h. The change of fluorescence intensity during the storage of FITC-MIP was also investigated (data not shown). When the FITC-MIP was stored for 31 d in a dark environment at 4 °C, the fluorescence intensity retained 92 % of its original response, which indicated that FITC-MIP has acceptable storage stability.

Conclusions

In summary, FITC was successfully incorporated into MIP as confirmed by FTIR spectrum and microscopy image. Based on photo-induced electron transfer

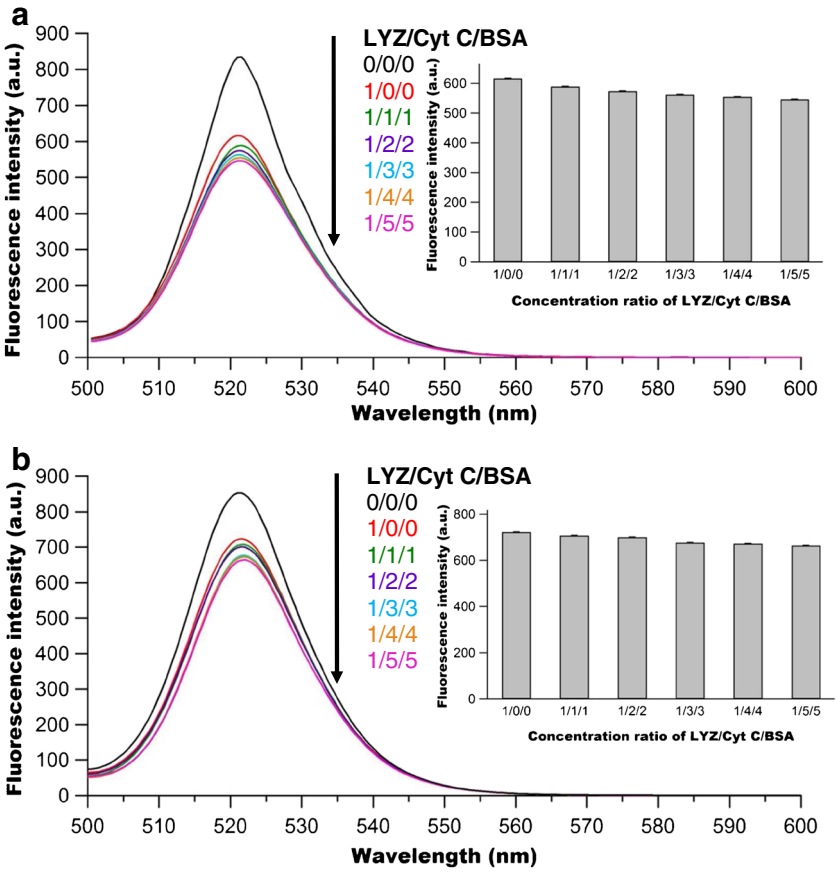

Fig. 9 Fluorescence emission spectra of the (**a**) FITC-MIP and (**b**) FITC-NIP with increasing concentration ratio of LYZ/Cyt C/BSA from 1/0/0 to 1/5/5 in PBS solution. The inset shows effect of competitive proteins on fluorescence quenching for respective samples. Adsorption condition: $V = 10$ mL, $W = 1.5$ mg, C_0, $_{LYZ} = 0.007$ mg mL^{-1}, temperature 25 °C, pH 10, time 1 h. The points represent mean values of three replicates of measurements and error bars represent standard errors

mechanism, the FITC-MIP could be successfully applied for direct, sensitive, and selective detection of LYZ. The fluorescence intensity of FITC-MIP decreased linearly with increasing LYZ in the concentration range of 0–0.025 mg mL^{-1} with a detection limit of 0.0015 mg mL^{-1}. It is found that LYZ can quench the fluorescence intensity of FITC-MIP in a concentration-dependent manner that is best described by a Stern-Volmer equation. Additionally, FITC-MIP demonstrated relatively fast binding kinetics because of the weak interactions (van der Waals forces and electrostatic forces) between the LYZ templates and polymer matrix. The experimental results also demonstrated that the fluorescence quenching efficiency of FITC-MIP for LYZ was much higher compared with other proteins (BSA and Cyt C). This illustrated that FITC-MIP possessed good selectivity towards template LYZ. Furthermore, the interference of competing proteins does not interfere with the fluorescence intensity of FITC-MIP significantly, implying highly selective recognition ability of the FITC-MIP, as it can detect the target LYZ from complex samples well. As a result, excellent stability as well as performance study suggest that FITC-MIP is a promising sensing material for biosensor in clinical diagnosis applications.

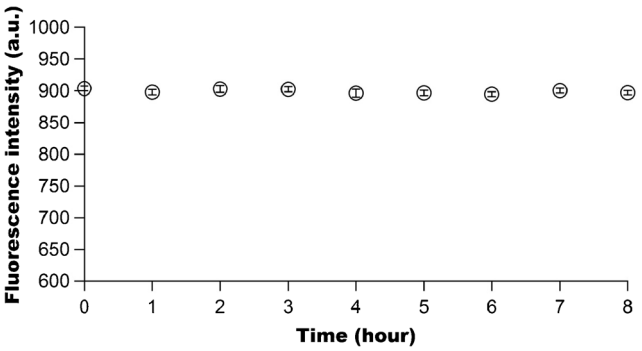

Fig. 10 Fluorescence intensity change of FITC-MIP within 8 h. The points represent average values of three replicate measurements and error bars represent standard errors

Acknowledgments This work is supported by Postgraduate Research Grant Scheme (grant no. 8046003), FRGS grant (6071271), and Research University Grant (814209). G.W.L. is financially assisted by MyPhD scholarship from the Ministry of Higher Education of Malaysia. All authors are affiliated with Membrane Science and Technology cluster USM.

Compliance with ethical standards

Conflict of interest The authors declare that there have no conflicts of interest.

References

1. Akinalp AS, Asan M, Ozcan N. Expression of T4 lysozyme gene (gene e) in *Streptococcus salivarius* subsp. *Thermophilus*. Afr J Biotechnol. 2007;6:963–6.
2. Li S, Mulloor JJ, Wang L, Ji Y, Mulloor CJ, Micic M, et al. Strong and selective adsorption of lysozyme on graphene oxide. ACS Appl Mater Interfaces. 2014;6:5704–12.
3. Ou SH, Wu MC, Chou TC, Liu CC. Polyacrylamide gels with electrostatic functional groups for the molecular imprinting of lysozyme. Anal Chim Acta. 2004;504:163–6.
4. Pascual R, Gee B, Finch S. Usefulness of serum lysozyme analysis in diagnosis and evaluation of sarcoidosis. N Engl J Med. 1973;289:1074–6.
5. Perillie PE, Kaplan SS, Lefkowitz E, Rogaway W, Finch SC. Studies of muramidase (lysozyme) in leukemia. J Am Med Assoc. 1968;203:317–22.
6. Osserman EF, Lawlor DP. Serum and urinary lysozyme (muramidase) in monocytic and monomyelocytic leukemia. J Exp Med. 1966;124:921–52.
7. Prockop DJ, Davidson WD. A study of urinary and serum lysozyme in patients with renal disease. N Engl J Med. 1964;270:269–74.
8. Fleming A. On a remarkable bacteriolytic element found in tissues and secretions. Proc R Soc Lond Ser B. 1922;93:306–17.
9. Newman J, Cacatian A, Josephson A, Tsang A. Spinal-fluid lysozyme in the diagnosis of central-nervous-system tumours. Lancet. 1974;304:756–7.
10. Ding Z, Annie Bligh SW, Tao L, Quan J, Nie H, Zhu L, et al. Molecularly imprinted polymer based on MWCNT-QDs as fluorescent biomimetic sensor for specific recognition of target protein. Mater Sci Eng C. 2015;48:469–79.
11. Rachkov A, McNiven S, El'skaya A, Yano K, Karube I. Fluorescence detection of β-estradiol using a molecularly imprinted polymer. Anal Chim Acta. 2000;405:23–9.
12. Zourob M. Recognition receptors in biosensors. New York: Springer Science Business Media; 2010.
13. Garcia R, Cabrita MJ, Costa Freitas AM. Application of molecularly imprinted polymers for the analysis of pesticide residues in food-A highly selective and innovative approach. Am J Anal Chem. 2011;2:16–25.
14. Fu G, He H, Chai Z, Chen H, Kong J, Wang Y, et al. Enhanced lysozyme imprinting over nanoparticles functionalized with carboxyl groups for noncovalent template sorption. Anal Chem. 2011;83:1431–6.
15. He H, Fu G, Wang Y, Chai Z, Jiang Y, Chen Z. Imprinting of protein over silica nanoparticles via surface graft copolymerization using low monomer concentration. Biosens Bioelectron. 2010;26:760–5.
16. Qian L, Hu X, Guan P, Wang D, Li J, Du C, et al. The effectively specific recognition of bovine serum albumin imprinted silica nanoparticles by utilizing a macromolecularly functional monomer to stabilize and imprint template. Anal Chim Acta. 2015;884:97–105.
17. Chen H, Yuan D, Li Y, Dong M, Chai Z, Kong J, et al. Silica nanoparticle supported molecularly imprinted polymer layers with varied degrees of crosslinking for lysozyme recognition. Anal Chim Acta. 2013;779:82–9.
18. Liu D, Yang Q, Jin S, Song Y, Gao J, Wang Y, et al. Core–shell molecularly imprinted polymer nanoparticles with assistant recognition polymer chains for effective recognition and enrichment of natural low-abundance protein. Acta Biomater. 2014;10:769–75.
19. Gai Q-Q, Qu F, Liu Z-J, Dai R-J, Zhang Y-K. Superparamagnetic lysozyme surface-imprinted polymer prepared by atom transfer radical polymerization and its application for protein separation. J Chromatogr A. 2010;1217:5035–42.
20. Jia X, Xu M, Wang Y, Ran D, Yang S, Zhang M. Polydopamine-based molecular imprinting on silica-modified magnetic nanoparticles for recognition and separation of bovine hemoglobin. Analyst. 2013;138:651–8.
21. Lee M-H, Thomas JL, Ho M-H, Yuan C, Lin H-Y. Synthesis of magnetic molecularly imprinted poly(ethylene-co-vinyl alcohol) nanoparticles and their uses in the extraction and sensing of target molecules in urine. ACS Appl Mater Interfaces. 2010;2:1729–36.
22. Li L, He X, Chen L, Zhang Y. Preparation of core-shell magnetic molecularly imprinted polymer nanoparticles for recognition of bovine hemoglobin. Chem Asian J. 2009;4:286–93.
23. Li Y, Yang H-H, You Q-H, Zhuang Z-X, Wang X-R. Protein recognition via surface molecularly imprinted polymer nanowires. Anal Chem. 2006;78:317–20.
24. Wang J, Gao L, Han D, Pan J, Qiu H, Li H, et al. Optical detection of λ-cyhalothrin by core-shell fluorescent molecularly imprinted polymers in chinese spirits. J Agric Food Chem. 2015;63:2392–9.
25. Sunayama H, Ooya T, Takeuchi T. Fluorescent protein recognition polymer thin films capable of selective signal transduction of target binding events prepared by molecular imprinting with a post-imprinting treatment. Biosens Bioelectron. 2010;26:458–62.
26. Zhao Y, Ma Y, Li H, Wang L. Composite QDs@MIP nanospheres for specific recognition and direct fluorescent quantification of pesticides in aqueous media. Anal Chem. 2012;84:386–95.
27. Wu X, Zhang Z, Li J, You H, Li Y, Chen L. Molecularly imprinted polymers-coated gold nanoclusters for fluorescent detection of bisphenol A. Sensors Actuators B: Chem. 2015;211:507–14.
28. Campbell PA, Canono BP, Drevets DA (2001) Measurement of bacterial ingestion and killing by macrophages. Current protocols in immunology. Hoboken NJ: John Wiley and Sons, Inc.; 2001.
29. Grunberg E, Cleeland R. Fluorescence and viability of proteus mirabilis stained directly with fluorescein isothiocyanate. J Bacteriol. 1966;92:23–7.
30. Miller JS, Quarles JM. Flow cytometric identification of microorganisms by dual staining with FITC and PI. Cytometry. 1990;11:667–75.
31. Kelly KA, Reynolds F, Weissleder R, Josephson L. Fluorescein isothiocyanate-hapten immunoassay for determination of peptide-cell interactions. Anal Biochem. 2004;330:181–5.
32. McClatchey KD. Clinical laboratory medicine. Philadelphia, PA: Lippincott Wiliams and Wilkins; 2002.
33. Huang J, Liu H, Men H, Zhai Y, Xi Q, Zhang Z, et al. Molecularly imprinted polymer coating with fluorescence on magnetic particle. Macromol Res. 2013;21:1021–8.
34. Chen L, Li J, Wang S, Lu W, Wu A, Choo J, et al. FITC functionalized magnetic core-shell Fe_3O_4/Ag hybrid nanoparticle for selective determination of molecular biothiols. Sensors Actuators B Chem. 2014;193:857–63.
35. Feng H, Wang N, Tran TT, Yuan L, Li J, Cai Q. Surface molecular imprinting on dye-(NH_2)-SiO_2 NPs for specific recognition and direct fluorescent quantification of perfluorooctane sulfonate. Sensors Actuators B Chem. 2014;195:266–73.
36. Stobiecka M, Chalupa A. Modulation of plasmon-enhanced resonance energy transfer to gold nanoparticles by protein survivin channeled-shell gating. J Phys Chem B. 2015;119:13227–35.
37. Stobiecka M. Novel plasmonic field-enhanced nanoassay for trace detection of proteins. Biosens Bioelectron. 2014;55:379–85.
38. Lim GW, Lim JK, Ahmad AL, Chan DJC. Molecularly imprinted polymer layers using *Navicula* sp. frustule as core material for selectively recognition of lysozyme. Chem Eng Res Des. 2015;101:2–14.
39. Fowler CE, Buchber C, Lebeau B, Patarin J, Delacôte C, Walcarius A. An aqueous route to organically functionalized silica diatom skeletons. Appl Surf Sci. 2007;253:5485–93.
40. Hildebrand M. Biological processing of nanostructured silica in diatoms. Prog Org Coat. 2003;47:256–66.

41. Yu Y, Addai-Mensah J, Losic D. Functionalized diatom silica microparticles for removal of mercury ions. Sci Technol Adv Mater. 2012;13:1–11.
42. Lemonas JF. Diatomite. Am Ceram Soc Bull. 1997;76:92–5.
43. Lim GW, Lim JK, Ahmad AL, Chan DJC. Influences of diatom frustule morphologies on protein adsorption behavior. J Appl Phycol. 2015;27:763–75.
44. Baumgärtel T, von Borczyskowski C, Graaf H. Selective surface modification of lithographic silicon oxide nanostructures by organofunctional silanes. Beilstein J Nanotechnol. 2013;4:218–26.
45. Bergmann NM (2005) Molecularly imprinted polyacrylamide polymers and copolymers with specific recognition for serum proteins. Ph.D. Dissertation, The University of Texas.
46. Pang S, Liu S, Su X. A novel fluorescence assay for the detection of hemoglobin based on the G-quadruplex/hemin complex. Talanta. 2014;118:118–22.
47. Tan L, Kang C, Xu S, Tang Y. Selective room temperature phosphorescence sensing of target protein using Mn-doped ZnS QDs-embedded molecularly imprinted polymer. Biosens Bioelectron. 2013;48:216–23.
48. Zhang C, Cui H, Cai J, Duan Y, Liu Y. Development of fluorescence sensing material based on CdSe/ZnS quantum dots and molecularly imprinted polymer for the detection of carbaryl in rice and chinese cabbage. J Agric Food Chem. 2015;63:4966–72.
49. Loucaides S, Behrends T, Van Cappellen P. Reactivity of biogenic silica: surface versus bulk charge density. Geochim Cosmochim Acta. 2010;74:517–30.
50. Tozak KÖ, Erzengin M, Sargın İ, Ünlü N. Sorption of DNA by diatomite-Zn (II) embedded supermacroporous monolithic p(HEMA) cryogels. EXCLI J. 2013;12:670–80.
51. Bergmann NM, Peppas NA. Configurational biomimetic imprinting for protein recognition: structural characteristics of recognitive hydrogels. Ind Eng Chem Res. 2008;47:9099–107.
52. Siyam T, Abd-Elatif ZH. Gamma radiation-induced preparation of poly(acrylamide-acrylic acid-dimethylaminoethylmethacrylate) as exchanger. J Macromol Sci. 1999;36:417–28.
53. Ghosh SK, Ali M, Chatterjee H. Studies on the interaction of fluorescein isothiocyanate and its sugar analogues with cetyltrimethylammonium bromide. Chem Phys Lett. 2013;561(562):147–52.
54. Jiang L, Li X, Liu L, Zhang Q. Cellular uptake mechanism and intracellular fate of hydrophobically modified pullulan nanoparticles. Int Jf Nanomed. 2013;8:1825–34.
55. Ma LY, Wang HY, Xie H, Xu LX. A long lifetime chemical sensor: study on fluorescence property of fluorescein isothiocyanate and preparation of pH chemical sensor. Spectrochim Acta A. 2004;60:1865–72.
56. Sjöback R, Nygren J, Kubista M. Absorption and fluorescence properties of fluorescein. Spectrochim Acta A. 1995;51:L7–21.
57. Harz S, Schimmelpfennig M, Tse Sum Bui B, Marchyk N, Haupt K, Feller K-H. Fluorescence optical spectrally resolved sensor based on molecularly imprinted polymers and microfluidics. Eng Life Sci. 2011;11:559–65.
58. Deng Q, Wu J, Zhai X, Fang G, Wang S. Highly selective fluorescent sensing of proteins based on a fluorescent molecularly imprinted nanosensor. Sensors. 2013;13:12994.
59. Verheyen E, Schillemans JP, van Wijk M, Demeniex M-A, Hennink WE, van Nostrum CF. Challenges for the effective molecular imprinting of proteins. Biomaterials. 2011;32:3008–20.